

A molecular dynamics study of Li-doped borate glasses

Ch.-P.E. Varsamis, A. Vegiri, E.I. Kamitsos

Theoretical and Physical Chemistry Institute,
National Hellenic Research Foundation,
48 Vas. Constantinou Ave., 11635 Athens, Greece

Received August 1, 2000

The objective of this work is to investigate the effect of alkali content and temperature on the microstructure of lithium borate glasses, $x\text{Li}_2\text{O} \cdot (1-x)\text{B}_2\text{O}_3$. We have applied the molecular dynamics technique with Ewald summation and periodic boundary conditions to a collection of ca. 256 particles confined within a primitive cubic cell and interacting through a Born-Mayer-Huggins type of potential augmented with three-body angular terms. The results of this study have been discussed in relation to experimental structural data obtained by NMR and infrared spectroscopies.

Key words: *molecular dynamics, lithium borate glasses*

PACS: *71.15.Pd, 61.43.Fs, 81.05.Kf*

1. Introduction

Ionic glasses constitute prominent probable materials for technological applications in electrochemical and optical devices [1–3]. The choice and design of the appropriate materials for specific applications require a detailed knowledge of their structure and physical properties. The lack of long range order in the glassy state limits the effectiveness of experimental techniques and theoretical calculations which work successfully when applied to crystalline materials. To overcome the difficulty, computational simulations may be employed to provide alternative ways of investigating microscopic and macroscopic properties of glasses [4–7].

The short-range order (SRO) structure of Li-borate glasses, $x\text{Li}_2\text{O} \cdot (1-x)\text{B}_2\text{O}_3$, at room temperature has been studied by NMR [8,9], mid-IR [10,11], Raman [12], and neutron diffraction [13] spectroscopies and by molecular dynamics simulations [5–7]. It is widely accepted that for Li_2O contents up to *ca.* $x = 0.25$ the transformation of neutral borate triangular units, BO_3 , into charged tetrahedral borate species, BO_4^- , constitutes the main modification mechanism of the short-range order (hereafter O will denote an oxygen atom bridging two boron centers) [8,10]. For x larger than *ca.* 0.25, borate triangles with non-bridging oxygen atoms (NBO's),

Table 1. Simulation parameters for $x\text{Li}_2\text{O} \cdot (1-x)\text{B}_2\text{O}_3$ glasses.

x	Number of atoms			R_{box} (Å)		
	B	O	Li	$T = 300$ K	$T = 600$ K	$T = 1200$ K
0.2	89	144	21	13.84	13.92	14.37
0.3	81	139	35	13.54	13.58	14.09
0.4	73	134	49	13.36	13.55	14.08
0.5	64	128	64	13.33	13.47	14.05

$\text{B}\text{O}_2\text{O}^-$, and BO_2^{2-} are formed and coexist with BO_4^- tetrahedra [14]. The effect of temperature on the SRO structure was investigated to a lesser extent. Statistical mechanics calculations [15] and NMR data [16] suggested that with increasing temperature conversion of BO_4^- tetrahedral into their isomeric $\text{B}\text{O}_2\text{O}^-$ species takes place [14].

The local environment of metal cations in borate glasses has been investigated by far-IR [10,11,17,18] and MD simulations [7]. In particular, the presence of two different cation hosting sites has been experimentally identified [10,11,17,18]. Questions regarding the tendency for aggregation of metal cations into clusters or their homogeneous distribution in the glass network constitute open challenges. In that respect, clustering models have been proposed, i.e. the cluster-tissue [19] and the modified random network model [20], as well as models assuming a homogeneous distribution of metal cations [21].

In this work, a molecular dynamics study of $x\text{Li}_2\text{O} \cdot (1-x)\text{B}_2\text{O}_3$ glasses is presented as a function of lithium oxide content, x , and temperature, T . The main emphasis of this work is to investigate the SRO structure and the local environments around Li ions and NBO's, and their distribution in the network, as a function of both x and T . The calculated SRO structure and the Li-site energetics have been compared with experimental NMR [8] and far-infrared [17,18] findings, respectively.

2. Computational procedure

Four different compositions in the $x\text{Li}_2\text{O} \cdot (1-x)\text{B}_2\text{O}_3$ glassy system were investigated at three temperatures by the molecular dynamics technique. In all simulations, structures consisting of ca. 256 atoms in a primitive cubic cell have been generated. The number of atoms used in each composition and the lattice constant of the unit cell, as determined from experimental densities [22,23], are summarized in table 1.

Interatomic interactions were treated by means of the usual Born-Mayer-Huggins potential:

$$V_{ij}(r) = A_{ij} \exp(-r/\rho) + z_i z_j e^2/r, \quad (1)$$

where

$$A_{ij} = 20.3545 \left(1 + \frac{z_i}{\eta_i} + \frac{z_j}{\eta_j} \right) \exp \left(\frac{r_i + r_j}{\rho} \right) \text{ (kJ/mol)}. \quad (2)$$

In equations (1) and (2), $z_i e$, η_i , r_i , are the charge, number of valence shell electrons and ionic radius, of ion i and ρ is the repulsion parameter ($\rho = 0.29 \text{ \AA}$).

An additional three-body harmonic interaction potential term for the O-B-O angles was included:

$$V_{ijk} = 0.5K_{ijk}(\theta - \theta_0)^2, \quad (3)$$

where K_{ijk} is a constant determining the strength of the interaction and θ is the angle between i-j and j-k bonds. The angle θ_0 corresponds to the potential energy minimum.

The potential model and the values of the parameters which appear in equations (1–3) have been taken from [7], where a partial scaling of the electrostatic charges necessary for the reproduction of the experimental IR [10,11] and Raman spectra [12], was adopted.

Our simulations have been carried out in the microcanonical ensemble, where the initial configuration was a random distribution of atoms over the sites of an fcc cubic lattice, with velocities taken from a Maxwellian distribution at 6000 K. Periodic boundary conditions were applied and long range Coulombic forces were handled by Ewald summation. A fifth-order Gear predictor-corrector integrator with a timestep of 0.96 fs was used. The generated melts were quenched to the final temperature in five cooling cycles. Each cycle consisted of a fast cooling step for about 2 ps and an equilibration period of about 10 ps. The equilibration period in the final cooling cycle was 30 ps, whereas properties were accumulated for a final period of about 60 ps.

3. Results and discussion

3.1. Short range order structure

The SRO structure of $x\text{Li}_2\text{O} \cdot (1-x)\text{B}_2\text{O}_3$ glasses with x values up to $x = 0.5$ was found to consist mainly of triangular borate, BO_3 and $\text{B}\text{O}_2\text{O}^-$, and tetrahedral, BO_4^- , units [8,10,11]. The mole fraction of tetrahedral BO_4^- units, X_4 , in the simulated glasses can be determined from the coordination number of B atoms calculated from the B-O radial distribution function. The mole fractions of $\text{B}\text{O}_2\text{O}^-$, X_2 , and $\text{B}\text{O}\text{O}_2^{2-}$ triangles, X_1 , were estimated by counting the number of NBOs per 3-coordinated boron center. An oxygen atom is identified as an NBO if no other boron atom is found in a sphere with a radius of *ca.* 2 Å. This distance corresponds to the first minimum of the B-O radial distribution function and was found to be independent of temperature and composition. The calculated fractions X_4 , X_2 and X_1 are listed in table 2.

Inspection of table 2 shows that the calculated charge per borate polyhedron center is systematically lower than that expected from stoichiometry. Such a difference can be attributed to the application of periodic boundary conditions that may transform an NBO situated close to the surface of the primitive cell into a bridging oxygen atom of a borate triangle. To eliminate such surface effects it is necessary to substantially increase the size of the system.

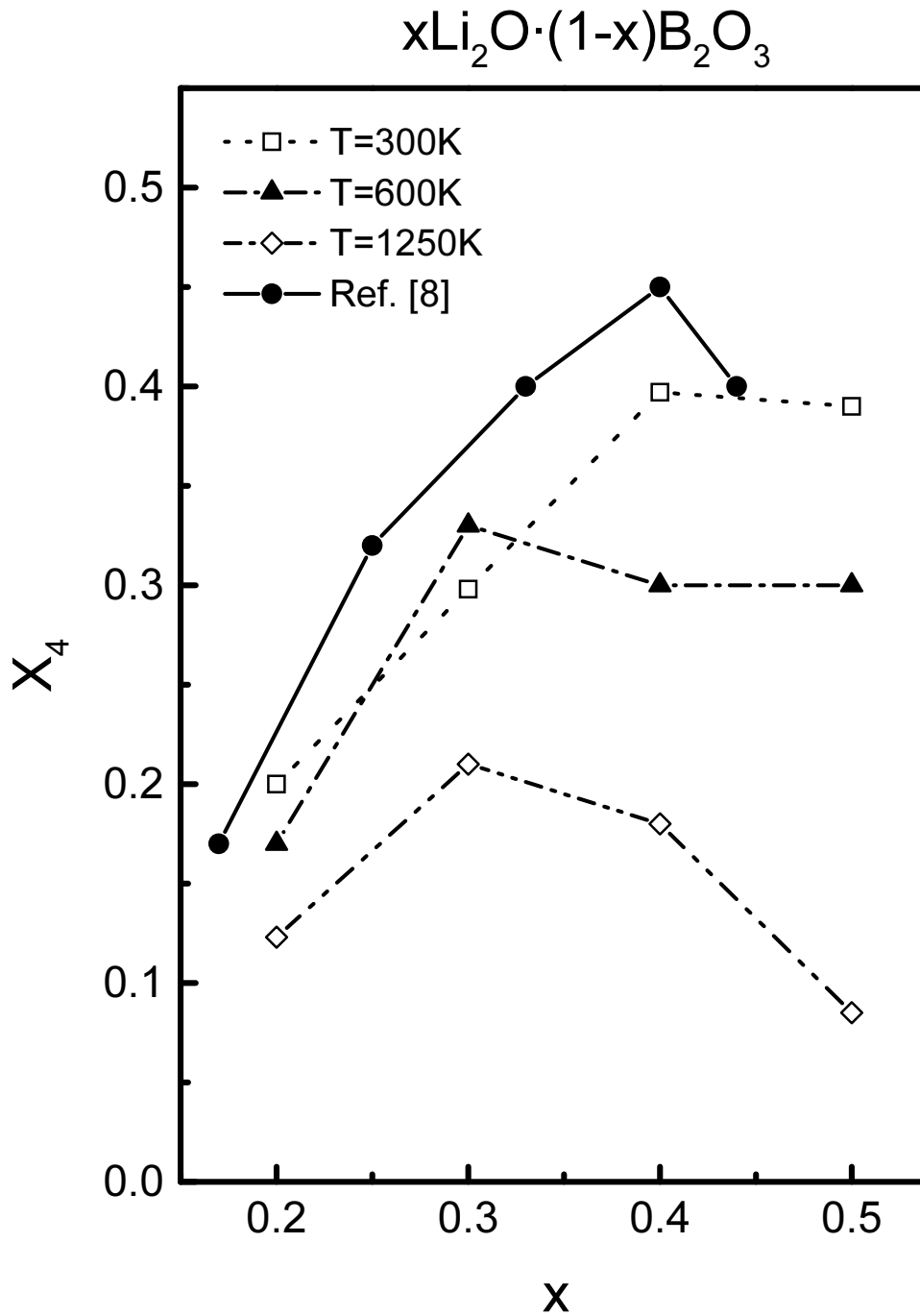


Figure 1. Calculated mole fractions of tetrahedral borate units, X_4 , at different compositions and temperatures, in $x\text{Li}_2\text{O} \cdot (1-x)\text{B}_2\text{O}_3$ glasses. Experimental X_4 values obtained from NMR room temperature study [8] at room temperature are also depicted for comparison.

Table 2. Mole fractions of $B\text{O}_4^-$, X_4 , $B\text{O}_2\text{O}^-$, X_2 , and $B\text{OO}_2^{2-}$, X_1 , units in $x\text{Li}_2\text{O} \cdot (1-x)\text{B}_2\text{O}_3$ glasses, as a function of lithium oxide mole fraction, x , and temperature, T . Calculated, $X_4 + X_2 + 2X_1$, and stoichiometric values, $x/(1-x)$, for the total negative charge per borate polyhedron are also reported.

T (K)	x	X_4	X_2	X_1	$X_4 + X_2 + 2X_1$	$x/(1-x)$
1250	0.2	12.3	5.1	0.8	19	25
	0.3	21	7.6	3.7	36	43
	0.4	18	18.7	8.4	53.5	66
	0.5	8.5	19.3	27.8	83.4	100
600	0.2	17	2.6	0	19.6	25
	0.3	33	7.5	0.8	42.1	43
	0.4	30	15.4	3.4	52.2	66
	0.5	30	14.5	11.9	68.3	100
300	0.2	20	2.4	0	22.4	25
	0.3	30	7.4	0	37.4	43
	0.4	40	11.1	2.3	55.7	66
	0.5	40	12.2	9.2	70.6	100

The calculated fractions X_4 at the three temperatures of the simulation are displayed in figure 1 versus Li_2O mole fraction. The experimental X_4 values obtained by NMR spectroscopy at 300 K [8], are also included for comparison. It is obvious that calculated X_4 fractions at 300 K are in close agreement with the experimental NMR values, whereas a systematic decrease of calculated X_4 with increasing temperature is observed. For charge conservation reasons, such a trend indicates the conversion of $B\text{O}_4^-$ units into triangular borate units with one or two NBOs. The isomerization of the energetically more stable tetrahedral $B\text{O}_4^-$ units into $B\text{O}_2\text{O}^-$ triangular species with increasing temperature has been predicted by Araujo with statistical mechanics calculations [15] and confirmed in high temperature NMR experiments by Stebbins and coworkers [16]. This finding is also consistent with the observed differences in the infrared and Raman spectra of alkali borate glasses having the same composition but different thermal histories, i.e. annealing treatment or cooling rates [24,25].

It is noted that the presence of $B\text{OO}_2^{2-}$ triangles in isolated pyroborate units, $B_2\text{O}_5^{4-}$, has been observed by infrared and Raman measurements at room temperature in the lithium borate glasses with $x \geq 0.5$ [10,12]. Our calculations at $T = 300$ K indeed show the formation of $B\text{OO}_2^{2-}$ units for $x \geq 0.4$. However, snapshots of the glass network indicate that $B\text{OO}_2^{2-}$ triangles are also found in the form of $B_2\text{O}_2\text{O}_3^{2-}$ and $B_2\text{O}_4^{3-}$ units, besides the isolated pyroborate moieties.

Representative snapshots of the glass structure at different compositions and temperatures are displayed in figures 2a,b. At low temperatures and compositions we observe the dominance of closed rings consisting of four, five or six boron atoms either in triangular or tetrahedral units. At larger alkali concentrations the closed rings become larger in size, whereas at $T = 1250$ K and $x = 0.5$ a considerable

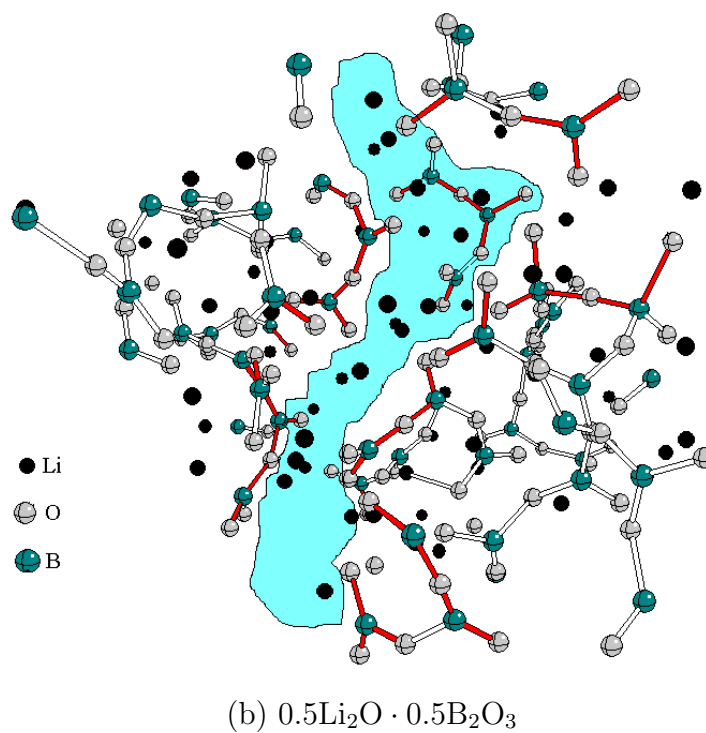
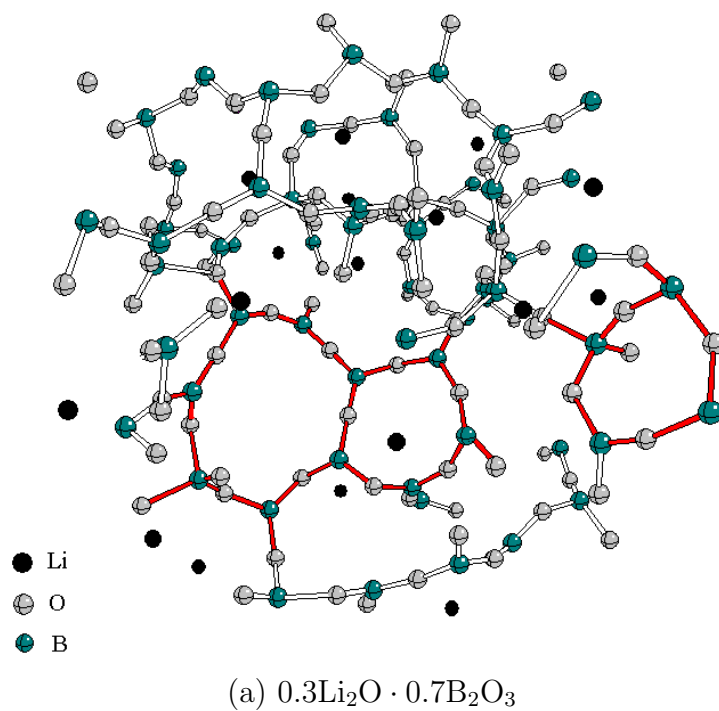


Figure 2. (a) Snapshot of the simulated structure for $0.3\text{Li}_2\text{O} \cdot 0.7\text{B}_2\text{O}_3$ glass at $T = 300$ K. Closed rings in the network structure are highlighted. (b) Snapshot of the simulated structure for $0.5\text{Li}_2\text{O} \cdot 0.5\text{B}_2\text{O}_3$ glass at $T = 1200$ K. The formation of ‘channels’ suitable for Li migration is highlighted.

Table 3. Distribution of Li-cations in $x\text{Li}_2\text{O} \cdot (1-x)\text{B}_2\text{O}_3$ glasses as a function of composition, x , and temperature, T . Li^{b} and Li^{nb} denotes Li cations in sites formed mainly by bridging (b-type) and non-bridging oxygen atoms (nb-type), respectively. Li^{m} denotes Li cations splitting their time between b-type and nb-type sites.

T (K)	x	% Li^{b}	% Li^{nb}	% Li^{m}
1250	0.2	47.6	23.8	28.6
	0.3	8.6	25.7	65.7
	0.4	0	89.6	10.4
	0.5	0	100	0
600	0.2	76.2	23.8	0
	0.3	40.0	37.1	22.9
	0.4	22.4	65.3	12.2
	0.5	18.7	64.1	17.2
300	0.2	71.4	19.1	9.5
	0.3	65.7	34.3	0
	0.4	42.9	46.9	10.2
	0.5	28.1	62.5	9.4

depolymerization of the glass network occurs with the prevalence of long, linear chains consisting mostly of triangular metaborate units ($\text{B}\text{O}_2\text{O}^-$).

3.2. Coordination environment of Li ions and non-bridging oxygen atoms

In order to investigate the nature of sites hosting metal cations we have distinguished Li cations according to the environments where they preferentially reside. A distinct Li-hosting site is identified if a Li cation spends more than 75 % of time in this particular site. Under this assumption, we were able to distinguish two types of Li-coordination environments: those formed primarily by bridging oxygen atoms in tetrahedral, BO_4^- , and neutral triangular units, BO_3 , (bridging-type, b-type environment) and those formed mainly by non-bridging oxygen atoms in charged $\text{B}\text{O}_2\text{O}^-$ or $\text{B}\text{O}\text{O}_2^{2-}$ triangles, and neutral triangular units (non-bridging-type, nb-type environment). Thus, a Li cation is designated by Li^{b} or Li^{nb} if it resides in a b-type or in nb-type environment, respectively. A Li cation is denoted mixed, Li^{m} , if it spends approximately half of its time in a b-type site and the other half of its time in an nb-type environment. We have good reasons to believe that Li cations in different types of sites do not behave in the same way, since they experience different micro-environments depending on composition and temperature. In table 3, we summarize the distribution of Li cations in the different local borate sites according to temperature and composition.

It is noted that the percentage of Li^{nb} increases monotonically with alkali content and temperature. This is consistent with the result that the fraction of NBO-

Table 4. Coordination numbers of NBO and O atoms and Li^{nb} cations in $x\text{Li}_2\text{O} \cdot (1-x)\text{B}_2\text{O}_3$ glasses as a function of composition, x , and temperature, T . For details see text.

T (K)	x	NBO(Li)	O(Li)	NBO(NBO)	$\text{Li}^{\text{nb}}(\text{Li}^{\text{nb}})$
1250	0.2	2.0	0.6	1.2	2.5
	0.3	2.3	1.1	1.5	3.1
	0.4	2.6	1.4	3.0	4.7
	0.5	2.9	2.2	5.2	6.7
600	0.2	2.2	0.6	0	1.3
	0.3	2.8	1.2	1.0	3.2
	0.4	3.0	1.8	2.4	5.4
	0.5	3.2	2.3	4.8	7.3
300	0.2	2.4	0.8	0	1.9
	0.3	2.6	1.1	0.6	2.5
	0.4	2.8	1.6	1.5	3.6
	0.5	3.05	2.1	2.0	5.7

containing units also increases with temperature and concentration (see table 2). However, it was found that the rate of increase of the percentage of Li^{nb} ions is greater than the corresponding rate of increase of NBOs. This finding can be explained if NBO atoms can coordinate with more than one Li cation. Along the same lines, the percentage of Li^{b} ions is systematically lower than the relative fraction of BO_4^- units, X_4 , with respect to all charged borate species, $X_4 + X_2 + X_1$. Thus, there is a preference of Li ions to coordinate with NBOs. For instance, at $T = 300$ K and $x = 0.4$ although the tetrahedral borate units represent 40 % of all charged and neutral local units in the system, or a 75 % of the charged units, the corresponding total Li^{b} percentage is 48 % , considering that half of Li^{m} ions reside in b-type sites. Such a trend becomes more pronounced at higher temperatures and concentrations; i.e., at $T = 1250$ K and $x = 0.4$ the mole fraction X_4 of BO_4^- units represents 40 % of the charged units, while 5 % of Li ions spend their time in b-type sites as Li^{m} cations. This is probably related with the increased kinetic energy of cations at $T = 1250$ K which now can more easily jump out of the shallower b-type wells than at $T = 300$ K.

Since the results of table 3 suggest that Li ions prefer to reside closer to NBO atoms, we will examine more thoroughly the region in the vicinity of an NBO atom. To this end, we calculate the coordination numbers of NBOs relative to all Li cations, $\text{NBO}(\text{Li})$, and to other NBOs, $\text{NBO}(\text{NBO})$. We also investigate the coordination numbers of Li^{nb} cations relative to NBOs, $\text{Li}^{\text{nb}}(\text{NBO})$ and to other Li^{nb} , $\text{Li}^{\text{nb}}(\text{Li}^{\text{nb}})$. The results are presented in table 4, as a function of composition and temperature. $\text{O}(\text{O})$ and $\text{Li}(\text{O})$ coordination numbers, not listed in this study, were found to be in close agreement with respect to those reported in the literature [7,13].

As seen in table 4, the average number of Li cations in the neighbourhood of

Table 5. Distribution of Li^{nb} cations in sites of different number of NBO atoms in $x\text{Li}_2\text{O} \cdot (1-x)\text{B}_2\text{O}_3$ glasses as a function of composition, x , and temperature T . Li_k^{nb} represents Li^{nb} cations residing in sites formed by k NBO atoms.

T (K)	x	Li_1^{nb}	Li_2^{nb}	Li_3^{nb}	Li_4^{nb}
1200	0.2	0.58	0.36	0.06	0
	0.3	0.6	0.31	0.09	0
	0.4	0.45	0.37	0.15	0.03
	0.5	0.17	0.29	0.30	0.18
300	0.2	1.00	0	0	0
	0.3	0.74	0.26	0	0
	0.4	0.75	0.25	0	0
	0.5	0.03	0.62	0.28	0.07

an NBO, $\text{NBO}(\text{Li})$, varies smoothly from *ca.* 2 to *ca.* 3 with increasing x , and is independent of temperature. The number of Li cations around an average oxygen atom, $\text{O}(\text{Li})$, is always smaller, varying between *ca.* 0.5 and 2. These findings imply that, indeed, there is an increased concentration of Li cations in sites formed by NBO atoms, in accord with the conclusions drawn from the previous discussion regarding the results of table 3. Such a behaviour can be attributed to stronger Coulombic interactions, and thus to the deeper potential wells that develop between Li ions and the more polarized NBO-containing sites, as compared to sites formed by oxygen atoms of tetrahedral units.

The calculated NBO-NBO correlation functions display two sharp and well-defined peaks, which correspond to NBO-atoms in the first shell. The first peak at a distance of 2.25 Å is attributed to NBO atoms belonging to the same unit, whereas the second peak at 3.31 Å is attributed to NBOs of neighbouring units. The $\text{NBO}(\text{NBO})$ coordination number of table 4 takes into account the contributions from both peaks and was found to increase with temperature and alkali concentration. In most cases these coordination numbers are significantly larger than unity, thus indicating the tendency of NBO atoms to agglomerate. Coordination numbers between 2 and 3 may be associated with the presence of NBO atoms in closed rings of the network structure. The larger coordination numbers found for the $x = 0.5$ composition, at $T = 600$ and 1250 K, fit better to a picture of a more open and depolymerized network consisting of “channels” suitable for ion migration [19,20].

Further support to the NBO agglomeration picture comes from the classification of Li^{nb} ions according to the percentage of time they spend in sites formed by a variable number of NBO atoms. In table 5 we present the distribution of residence times of Li^{nb} ions found in sites with 1 (Li_1^{nb}), 2 (Li_2^{nb}), 3 (Li_3^{nb}), or 4 (Li_4^{nb}) NBO atoms, averaged over all Li^{nb} ions. The probability to find a Li^{nb} atom in sites with more than one NBOs increases with temperature and Li-concentration. The crucial role of cation hosting sites formed by more than one NBOs in ionic transport properties has been reported in a recent theoretical study in Li-phosphate glasses

[26]. In particular, it was shown that Li_3^{nb} cations are characterized by the lowest activation energy necessary to hop into an adjacent site. In the same direction, we are currently exploiting the role of NBOs to the diffusion properties of Li cations in borate glasses.

3.3. Manifestation of Li-environments on the Li-O vibrational spectra

The discrimination of different cation hosting sites, e.g. b-type and nb-type environments, can be correlated with the corresponding Li-O vibrations which are active in the far-IR spectral range. In fact, far-IR experimental spectra are characterized by an asymmetric absorption profile, which can be adequately simulated with two Gaussian component bands [10,11,17,18]. Such an example is shown in figure 3a for the $0.3\text{Li}_2\text{O} \cdot 0.7\text{B}_2\text{O}_3$ glass [17,18]. The two component bands designated by L (254 cm^{-1}) and H (419 cm^{-1}) have been attributed to Li-O vibrations in sites characterized by different coordination numbers/charge density. In particular, the H band was associated with Li-O vibrations in sites of larger anionic charge density/smaller coordination number, while the L band was attributed to vibrations of Li cations in energetically less favourable sites (smaller charge density/larger coordination number) [17,18]. It is noted that absorption at frequencies above *ca.* 500 cm^{-1} is mainly attributed to vibrational modes of the borate network.

In view of the results of the present molecular dynamics study it is of great interest to further examine the microscopic origin of the L and H Li-O vibrational bands. For this purpose we calculated the velocity autocorrelation function, $\Phi(t)$, which corresponds to Li^{nb} and Li^{b} cations:

$$\Phi(t) = \left\langle (1/N) \sum_{j=1}^N \vec{v}_j(t) \cdot \vec{v}_j(0) \right\rangle, \quad (4)$$

where $\vec{v}_j(t)$ is the velocity of ion j at time t and N is the total number of Li^{nb} or Li^{b} ions. The vibrational density of states, $\Phi(\omega)$, which reflects the vibrational properties of Li cations, is obtained from the Fourier transform of $\Phi(t)$.

A representative example of calculated $\Phi(\omega)$ spectra is given in figure 3b for the $x = 0.3$ composition ($T = 300\text{ K}$) and compared with the experimental far-infrared spectrum of the same glass. It is evident that the $\Phi(\omega)$ spectra of Li^{nb} and Li^{b} cations are well distinguished from each other, with the Li^{b} spectrum shifted to lower frequencies. This result is probably due to the fact that the charge density of b-type environments is more delocalized compared to that of nb-type sites, resulting to lower anionic charge density and consequently to lower values of Li-O vibration frequencies. Comparison of the $\Phi(\omega)$ spectra with the deconvoluted experimental spectrum of the Li-borate glass suggests that it is plausible to assign the experimental L and H component bands to Li-O vibrations mostly in b-type and nb-type environments, respectively. In addition, the best fit of the experimental spectrum produced by a linear combination of the calculated $\Phi(\omega)$ spectra of Li^{nb} and Li^{b} ions is also displayed in figure 3b and shows good agreement with the experimental spectrum below *ca.* 500 cm^{-1} where the Li-O vibrations are active.

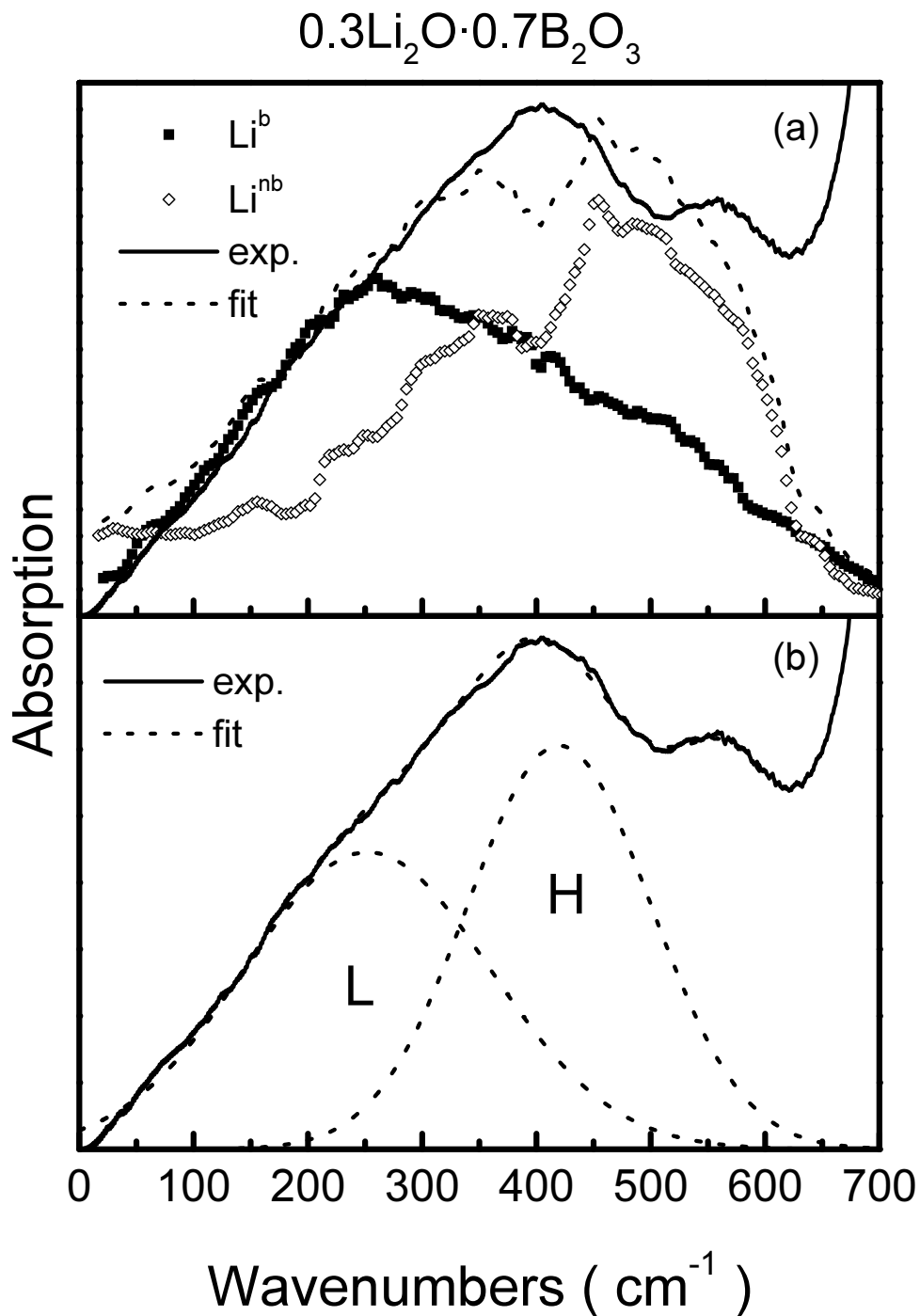


Figure 3. (a) Experimental far-infrared spectrum of $0.3\text{Li}_2\text{O} \cdot 0.7\text{B}_2\text{O}_3$ glass [18]. (b) Calculated power spectra, $\Phi(\omega)$, of Li ions residing in non-bridging oxygen-type, Li^{nb} , and bridging oxygen-type, Li^{b} , sites for the $0.3\text{Li}_2\text{O} \cdot 0.7\text{B}_2\text{O}_3$ glass at $T = 300$ K. A linear combination of the $\Phi(\omega)$ spectra of Li^{b} and Li^{nb} ions is also shown for comparison with the experimental spectrum in (a). Note the close correspondence of L and H bands with the power spectrum of Li^{b} and Li^{nb} cations, respectively.

4. Conclusions

The effect of alkali content and temperature on the structure of lithium borate glasses, $x\text{Li}_2\text{O} \cdot (1-x)\text{B}_2\text{O}_3$, has been investigated by molecular dynamics simulations. Room temperature results concerning the mole fractions of local borate units are in good agreement with the experimental NMR and IR results. Temperature increase was found to result in the decrease of the mole fraction of BO_4^- tetrahedral units in favour of charged borate triangles, BO_2O^- and BOO_2^{2-} , for all compositions. This is in agreement with statistical mechanics and high-temperature NMR results.

Li cations were found to explore two distinct environments, non-bridging oxygen-type and bridging oxygen-type sites, formed primarily by NBO atoms and oxygen atoms in tetrahedral borate units, respectively. A preference of Li ions to reside close to non-bridging oxygen atoms, as well as a tendency for non-bridging oxygen atoms to aggregate with increasing temperature and alkali content was found. For glasses of high alkali content ($x = 0.5$) it was shown that lithium cations cluster around NBO atoms and form “channels” through the glass network, in agreement with the cluster-tissue and modified random network models.

The distinction of cations into two types, Li^{nb} and Li^{b} for cations occupying nb-type and b-type sites, respectively, is very well reflected on their spectral properties. The calculated power spectra of Li^{nb} are peaking at higher frequencies compared to those of Li^{b} ions. This is in accord with the analysis of two component bands in the experimental far-infrared spectra, attributed to Li-O vibrational modes in different anionic sites.

5. Acknowledgements

This work was supported by EU through the INTAS 99-01162 Program and in part by the Greek General Secretariat for Research and Technology (PENED99-99ED44).

References

1. Ingram M.D. Ionic conductivity in glass. // *Phys. Chem. Glasses*, 1987, vol. 28, No. 6, p. 215–234.
2. Minami T. Recent progress in superionic conducting glasses. // *J. Non-Cryst. Solids*, 1987, vol. 95&96, p. 107–118.
3. Ingram M.D. Superionic glasses: theories and applications. // *Current Opinion in Solid State and Materials Science*, 1997, vol. 2, p. 399–404.
4. Inoue H., Aoki N., Yasni I. Molecular dynamics simulation of the structure of borate glasses. // *J. Am. Ceram. Soc.*, 1987, vol. 70, No. 6, p. 622–627.
5. Soppe W., Van der Marel C., Den Hartog H. W. Structural and dynamical properties of some lithium borate glasses. // *J. Non-Cryst. Solids*, 1988, vol. 101, p. 101–110.
6. Soppe W., Den Hartog H.W. A molecular dynamics study of $(\text{B}_2\text{O}_3)_{1-x-y}(\text{Li}_2\text{O})_x(\text{Li}_2\text{Cl}_2)_y$ and $(\text{B}_2\text{O}_3)_{1-x-y}(\text{Li}_2\text{O})_x(\text{Cs}_2\text{O})_y$. // *J. Non-Cryst. Solids*, 1989, vol. 108, p. 260–268.

7. Verhoef A.H., Den Hartog H.W. Structure and dynamics of alkali borate glasses: a molecular dynamics study. // *J. Non-Cryst. Solids*, 1995, vol. 182, p. 235–247.
8. Zhong J., Bray P.J. Change in Boron coordination in alkali borate glasses and mixed alkali effects, as elucidated by NMR. // *J. Non-Cryst. Solids*, 1989, vol. 111, p. 67–76.
9. Ratai E., Janssen M., Eckert H. Spatial distributions and chemical environments of cations in single- and mixed alkali borate glasses: Evidence from solid state NMR. // *Solid State Ionics*, 1998, vol. 105, p. 25–37.
10. Kamitsos E.I., Patsis A.P., Karakassides M.A., Chryssikos G.D. Infrared reflectance spectra of lithium borate glasses. // *J. Non-Cryst. Solids*, 1990, vol. 126, p. 52–67.
11. Verhoef A.H., Den Hartog H.W. Infrared spectroscopy of network and cation dynamics in binary and mixed alkali borate glasses. // *J. Non-Cryst. Solids*, 1995, vol. 182, p. 221–234.
12. Kamitsos E.I., Karakassides M.A., Chryssikos G.D. A vibrational study of Li-borate glasses with high Li₂O content. // *Phys. Chem. Glasses*, 1987, vol. 28, p. 203–209.
13. Swenson J., Borjesson L., Howells W.S. Structure of borate glasses from neutron-diffraction experiments. // *Phys. Rev. B*, 1995, vol. 52, No. 13, p. 9310–9318.
14. Kamitsos E.I., Chryssikos G.D. Borate glass structure by Raman and infrared spectroscopies. // *J. Mol. Structure*, 1991, vol. 247, p. 1–16.
15. Araujo R.J. Statistical mechanics of chemical disorder: Application to alkali borate glasses. // *J. Non-Cryst. Solids*, 1983, vol. 58, p. 201–208.
16. Stebbins J.F., Sen S., George A.M. High temperature nuclear magnetic resonance studies of oxide melts. // *J. Non-Cryst. Solids*, 1995, vol. 192&193, p. 298–305.
17. Kamitsos E.I., Patsis A.P., Chryssikos G.D. Infrared reflectance spectra of alkali diborate glasses. // *J. Non-Cryst. Solids*, 1993, vol. 152, p. 246–255.
18. Kamitsos E.I., Chryssikos G.D. Alkali sites in glass. // *Solid State Ionics*, 1998, vol. 105, p. 75–85.
19. Ingram M.D., Mackenzie M.A., Muller W, Torge M. Cluster and pathways: A new approach to ion migration in glass. // *Solid State Ionics*, 1988, vol. 28–30, p. 677–680.
20. Greaves G.N. EXAFS glass structure and diffusion. // *Phil. Mag. B*, 1989, vol. 60, No. 6, p. 793–800.
21. Swenson J., Borjesson L. Correlation between free volume and ionic conductivity in fast ion conducting glasses. // *Phys. Rev. Lett.*, 1996, vol. 77, No. 17, p. 3569–3572.
22. Feller S. et al. A review of the relationship between structure and physical properties in alkali borosilicate glasses. // *Borate glasses crystals and melts*, Proc. of the 2nd Inter. Conf. on Borate Glasses, Crystals and Melts. Oxford, UK, Society of Glass Technology, 1997, p. 246–253.
23. Mazurin O.V., Streltsina M.V. *Handbook of Glass Data. Part B.* New York, Elsevier, 1985.
24. Kamitsos E.I., Karakassides M.A. Effect of melt temperature on glass structure. // *Phys. Chem. Glasses*, 1989, vol. 30, No. 6, p. 235–236.
25. Varsamis C.P., Kamitsos E.I., Chryssikos G.D. Structure of fast-ion conducting AgI-doped borate glasses in bulk and thin film forms. // *Phys. Rev. B*, 1999, vol. 60, No. 6, p. 3885–3898.
26. Karthikeyan A., Vinatier P., Lévassieur A., Rao K.J. The molecular dynamics study of lithium ion conduction in phosphate glasses and the role of non-bridging oxygen. // *J. Phys. Chem. B*, 1999, vol. 103, p. 6185–6192.

Дослідження боратного скла легованого літєм методом молекулярної динаміки

Ч.-П.Е. Варсаміс, А. Вегірі, Е.І. Камітсос

Інститут теоретичної і фізичної хімії,
11635 Афіни, Греція

Отримано 1 серпня 2000 р.

Метою даної роботи є дослідження впливу лужного вмісту і температури на мікроструктуру $x\text{Li}_2\text{O} \cdot (1-x)\text{B}_2\text{O}_3$. Ми застосували метод молекулярної динаміки з пересумовуванням за Евальдом до набору з 256 частинок, розміщених в примітивній кубічній комірці, що взаємодіють з потенціалом типу Борна-Майєра-Хаггіна, доповненим членами тричастинкової кутової взаємодії. Результати цих досліджень обговорюються в зв'язку з експериментальними даними, отриманими методами ядерного магнітного резонансу і інфрачервоної спектроскопії.

Ключові слова: молекулярна динаміка, боратне скло

PACS: 71.15.Pd, 61.43.Fs, 81.05.Kf